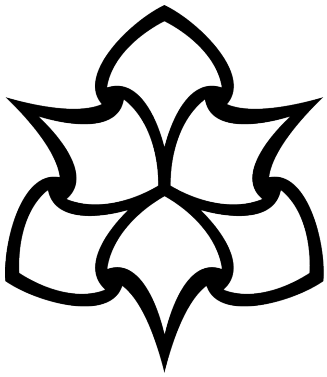

Biomacromolecules

pubs.acs.org/Biomac

Article

Aromatic Stacking Facilitated Self-Assembly of Ultrashort Ionic Complementary Peptide Sequence: β-Sheet Nanofibers with Remarkable Gelation and Interfacial Properties

Jacek K. Wychowaniec, Ronak Patel, James Leach, Rachel Mathomes, Vikesh Chhabria, Yogita Patil-Sen, Araida Hidalgo-Bastida, Robert T. Forbes, Joseph M. Hayes, and Mohamed A. Elsawy*

Cite This: https://dx.doi.org/10.1021/acs.biomac.0c00366

Read Online

ACCESS | Metrics & More | Article Recommendations | Supporting Information

ABSTRACT: Understanding peptide self-assembly mechanisms and stability of the formed assemblies is crucial for the development of functional nanomaterials. Herein, we have adopted a rational design approach to demonstrate how a minimal structural modification to a nonassembling ultrashort ionic self-complementary tetrapeptide *FEFK* (Phe4) remarkably enhanced the stability of self-assembly into β-sheet nanofibers and induced hydrogelation. This was achieved by replacing flexible phenylalanine residue (*F*) by the rigid phenylglycine (*Phg*), resulting in a constrained analogue *Phg*E*Phg*K (Phg4), which positioned aromatic rings in an orientation favorable for aromatic stacking. Phg4 self-assembly into stable β-sheet ladders was facilitated by π-staking of aromatic side chains alongside hydrogen bonding between backbone amides along the nanofiber axis. The contribution of these noncovalent interactions in stabilizing self-assembly was predicted by in silico modeling using molecular dynamics simulations and semiempirical quantum mechanics calculations. In aqueous medium, Phg4 β-sheet nanofibers entangled at a critical gelation concentration ≥20 mg/mL forming a network of nanofibrous hydrogels. Phg4 also demonstrated a unique surface activity in the presence of immiscible oils and was superior to commercial emulsifiers in stabilizing oil-in-water (O/W) emulsions. This was attributed to interfacial adsorption of amphiphilic nanofibrils forming nanofibrilized microspheres. To our knowledge, Phg4 is the shortest ionic self-complementary peptide rationally designed to self-assemble into stable β-sheet nanofibers capable of gelation and emulsification. Our results suggest that ultrashort ionic-complementary constrained peptides or UICPs have significant potential for the development of cost-effective, sustainable, and multifunctional soft bionanomaterials.

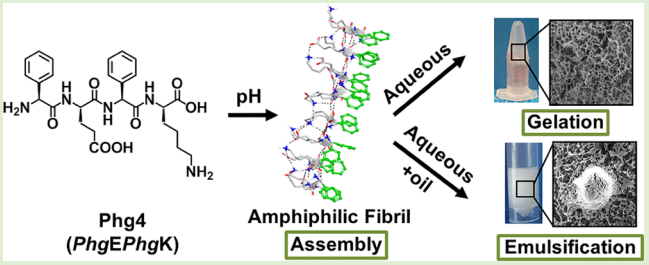

INTRODUCTION

Molecular self-assembly has been exploited in nature for the engineering of complex higher macromolecular structures of the proteome. Inspired by nature, the bottom-up design of de novo self-assembling peptides has been extensively investigated in the last three decades to innovate a wide variety of stable nanostructures for biomedical applications.[1,2] Zhang and co-workers were the first to propose the self-assembling ionic self-complementary peptide sequence pattern, with alternation of hydrophobic (A) and hydrophilic charged (B) amino acids: $(ABAB)_n$, where *n* is the number of the pattern repeats.[3,4] This design was inspired by the unusual sequence pattern EAK16 identified in a segment of the Z-DNA binding protein Zuotin, which was purified from the nuclear extract of the baker's yeast *Saccharomyces cerevisiae*.[5]

Peptides based on this sequence pattern were shown to self-assemble into stable β-sheet nanofibers, with typically ∼8−16 residues (n = 2−4) required to maintain the thermodynamic stability of the assembled nanostructures.[3,4,6−13] Interestingly, the tetrapeptide *FEFK* (Phe4), which is the shortest reported sequence with the ABAB pattern (n = 1), failed to self-assemble into stable β-sheet structures, implicating the importance of the sequence length for the stability of the formed assemblies (Figure 1A).[8,9] This could possibly be attributed to the fact that longer sequences provide more backbone amide bonds readily available for intermolecular hydrogen bonding between peptide chains, stabilizing the assembled β-sheet structures.

Herein, we investigated whether the structural modification of Phe4 to the more constrained phenylglycine based analogue Phg4 (Figure 1B) would lead to self-assembly into stable amphiphilic β-sheet fibers in aqueous medium and formation of a hydrogel. Our hypothesis was that the introduction of the rigid phenylglycine (*Phg*) residue would result in a more

Received: March 11, 2020
Revised: May 12, 2020
Published: May 13, 2020

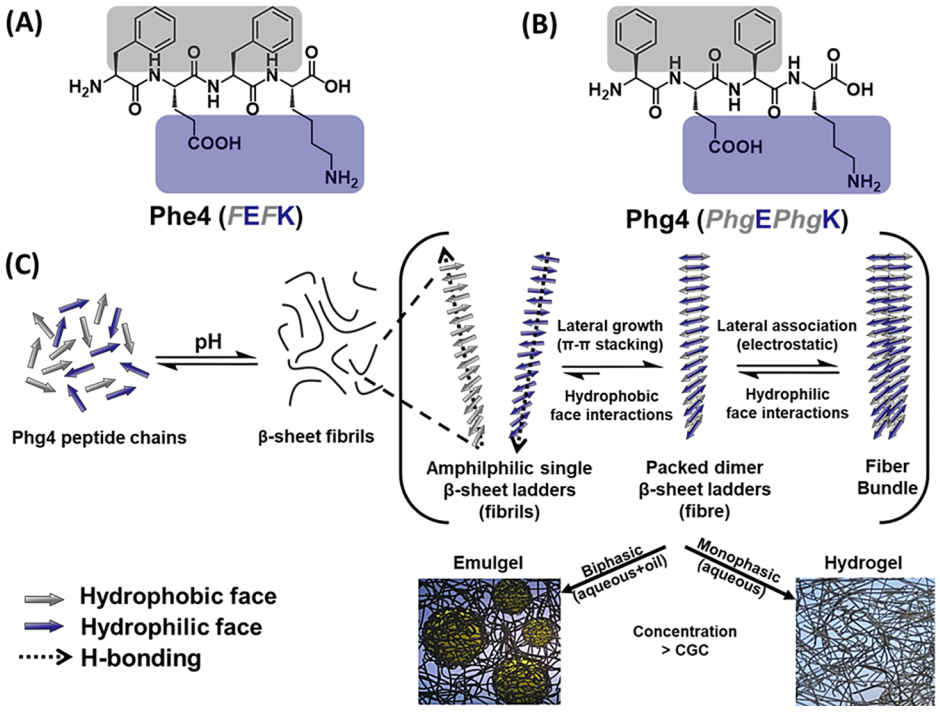

Figure 1. Molecular structures of (A) Phe4 (*FEFK*) and (B) Phg4 (*Phg*E*Phg*K) peptides. (*F*, phenylalanine; E, glutamic acid; K, lysine; *Phg*, phenylglycine). (C) Schematic illustration of Phg4 self-assembly into the amphiphilic *β*-sheet single ladder form, though *π*-stacking of the aromatic rings alongside the intermolecular hydrogen bonding between backbone amides. The single ladder form is in equilibrium with the more thermodynamically stable packed *β*-sheet ladders in aqueous medium, where the latter is formed by lateral growth through hydrophobic interactions of the aromatic rings projecting from the hydrophobic face. In monophasic medium, the packed form is more abundant forming nanofibers, which above critical gelation concentration (CGC) entangle into a nanofibous network forming hydrogels. In oil−water biphasic media, the amphiphilic single ladder will adsorb on the oil−water interface forming oil-in-water (O/W) emulgel (EMG). The hydrophobic face is denoted by gray color and the hydrophilic by violet.

constrained sequence with the aromatic rings directly attached to the peptide backbone readily positioned for intermolecular *π*-staking (Figure 1B). This will help stabilize the assembled peptide chains alongside hydrogen bonds formation between the chains backbone amides along the fiber axis, forming a stable amphiphilic *β*-sheet ladder (Figure 1C).[14,15] A single ladder will in turn interact with a second one through lateral *π*-interactions of the aromatic rings, which become packed between the dimer ladders shielding the hydrophobic faces from the surrounding aqueous medium (Figure 1C). Further lateral growth of the packed fibers can happen through the possible electrostatic interaction between the exposed charged E and K residues side chains, forming thicker fiber bundles (Figure 1C). To rationalize the observed effectiveness of Phg4 self-assembly at the atomic level and confirm the role of the aforementioned noncovalent interactions in stabilizing self-assembly, we have performed in silico modeling on the packed dimer ladder in the form of Prime minimization and side chain predictions, molecular dynamics (MD) simulations, and semiempirical quantum mechanics (SQM) calculations.

We have also investigated the interfacial activity of the unpacked amphiphilic *β*-sheet ladder, which is in thermodynamic equilibrium with the packed form, for stabilizing oil-in-water (O/W) emulgels (EMGs) in biphasic media (Figure 1C).[16−19] EMGs stability was tested versus a number of commercial emulsifiers under a range of environmental and storage conditions. For these investigations, a variety of techniques were used for the molecular, mesoscopic, macroscopic, and mechanical characterizations of both hydrogels and EMGs; mainly including Fourier transform infrared spectroscopy (FTIR), scanning electron microscopy (SEM), transmission electron microscopy (TEM), atomic force microscopy (AFM), small-angle X-ray scattering (SAXS), and oscillatory shear rheology.

We have demonstrated the importance of understanding the mechanisms of peptide self-assembly and stability of the assembled structures at a molecular level, which are of paramount importance for the rational engineering of peptide based nanomaterials.

MATERIALS AND METHODS

Materials. The Phe4 (*FEFK*) and Phg4 (*Phg*E*Phg*K) peptides were purchased from Cambridge Reagents Ltd. with ≳95% purity, as estimated by HPLC (Figure S1). Melissa oil was acquired from Essential Oils Direct Ltd. Sodium dodecyl sulfate (SDS), sodium chloride, potassium phosphate monobasic, and potassium thiocyanate were purchased from Acros Organics with a purity of ≥99%. Potassium chloride was procured form Alfa Aesar. Polysorbate 80 (Tween 80; 99%), poly(ethylene glycol)-*block*-poly(propylene glycol)-*block*-poly(ethylene glycol)/poloxomer (Pluronic F-68; 99%), and alkyltrimethylammonium bromide (cetrimide; ≥95%) were obtained from Sigma-Aldrich. HPLC grade water and chloroform were supplied by Thermo Fisher.

Computational Details. Initial models of single chain Phg4 and an antiparallel amphiphilic packed dimer *β*-sheet ladder model composed of 16 Phg4 peptide chains (2 × 8) were built using Maestro and Protein Preparation Wizard,[20] with the protonation states assigned on the basis of PROPKA[21] at pH 7.0. To design these initial models, the solved structure of an amyloid forming peptide KLVFFA from amyloid beta (PDB code 3OW9) was used as a scaffold for editing to Phg4. Different alignments and conformations of the phenyl side chains were manually explored in terms of the

https://dx.doi.org/10.1021/acs.biomac.0c00366
Biomacromolecules XXXX, XXX, XXX−XXX

potential association between the two sheets in the packed dimer, considering favorable π-stacking distances and nonpolar C−C, C−H, and H−H van der Waals distances that are in the attraction region.[22,23] Prime v4.5[20] minimizations and side chain predictions were performed on the starting models.[24] For the latter, rotamer libraries were used for random side chain adjustments together with minimizations, until the side chain rotamers were converged. The OPLS3 force field was used and water solvation effects accounted for using the implicit variable-dielectric generalized Born model (VSGB), which incorporates residue dependent effects.[25,26] Single chain Phg4 and the packed dimer model of Phg4 then underwent Desmond v4.7[20,27] 100 ns MD simulations in the NPT ensemble again with the OPLS3 force field but water solvation effects now explicitly accounted for using the TIP3P model. Three independent MD simulations were performed for the packed dimer using different seeds for assignment of the initial velocities and the trajectory postprocessed packed-dimer energies, again using Prime. Full details of the simulations and postprocessing are given in the Supporting Information. Following the dynamics, single chain and peptide aggregation geometries from the trajectories (three simulations combined for the packed dimer) were clustered into the recommended number of clusters (20 and 31 for single chain and packed dimer, respectively) based on atomic RMSDs (heavy atoms) and the affinity propagation method.[28] The representative structures from each group were then considered in SQM PM7 optimizations using a restricted Hartree−Fock (RHF) wave function and molecular mechanics correction to CONH bonds (MMOK setting).[29] All optimizations included the COSMO implicit solvation model (conductor-like screening model) with a dielectric constant of 78.4 for water.[30,31] The Localized Molecular Orbitals method available in MOPAC in the form of the linear scaling SCF MOZYME algorithm was used to speed up calculations.[32,33] Models with the lowest heats of formation were considered for further analyses. The SQM calculations were performed using MOPAC2016.[34]

Preparation of Hydrogels. Peptide powder was dissolved in HPLC water under vortex at 2500 rpm for 1 min. To trigger self-assembly and gelation the pH was then adjusted to ∼4.5−5 by stepwise addition of 0.5 M NaOH solution, while agitation for 30−60 s in between additions. After pH adjustment, the final volume was corrected using HPLC water to obtain the required concentration. Hydrogels were left in fridge at 4 °C overnight to equilibrate and used the following day.

Preparation of Emulsions and Emulgels. The oil phase (either chloroform or Melissa) was added dropwise to the peptide aqueous phase of pH values preadjusted separately to ∼2, 4.5−5, or 8.6 (by stepwise addition of 0.5 M NaOH solution as detailed under preparation of hydrogel), with mixing for 30 s in between additions at 2500 rpm using vortex. Different volumes of the oil phase were added to obtain W:O volume ratios of 2:8, 7:3, 6:4, 5:5, 4:6, 3:7, and 8:2.

Stability Testing of Emulsions and Emulgels. The stability of the emulgels (EMGs) with Melissa oil phase (EMG-M) formulation was compared with the traditional surfactants; SDS, poloxomer (Pluronic F-68), cetrimide, and Tween 80 all used at 50 mM and W:O ratio of 7:3. Three different conditions were investigated; long-term stability (5 weeks), thermostability at 60 °C for 3 h (in a Gallenkamp Hotbox oven with fan), and salt-stability using sodium chloride, potassium phosphate monobasic, and potassium thiocyanate salts at 100 mM for 1 week. For the perpetration of formulations for salt-stability, the peptide and surfactants were dissolved straight into the salt solutions instead of HPLC water. Additionally, the long-term stability (10 weeks) of EMG-M with different W:O volume ratios (2:8, 3:7, 4:6, 5:5, 6:4, 7:3, and 8:2) at a peptide concentration of 30 mg/mL was examined. With the exception of the thermostability analysis, all gels were incubated at room temperature (25 °C).

Attenuated Total Reflectance−Fourier Transform Infrared Spectroscopy (ATR-FTIR). Hydrogels and EMG preparations were spread onto the crystal of a Thermo Nicolet IR200 spectrophotometer to evaluate the peptide secondary structure. Transmittance was recorded between 4000 and 400 cm^{-1} at 128 scans, with a resolution of 2 cm^{-1}. HPLC water was used as background, which was automatically subtracted from the sample spectra by OMNIC software provided with the instrument.

Fluorescence Thioflavin T (ThT) Assay. ThT assay was performed using fluoroSENS spectrofluorometer (GILDEN photonics). ThT was mixed in 20 mg/mL of both peptide solutions/hydrogels during their preparation with a final 5 μM concentration, and these were either left at the pH before titration (with their pH measured as ∼2−2.3) or titrated using 0.5 M NaOH to a pH value of 4.5. Excitation wavelengths used were 400 and 450 nm, and the fluorescence scan range was set to 460−600 nm.

Oscillatory Rheology. A stress-controlled Discovery Hybrid Rheometer HR-2 (TA Instruments) was used to measure the rheological properties of the hydrogels and EMGs using a 20 mm Peltier plate with a parallel plate geometry and equipped with solvent trap to minimize evaporation. A sample of 500 μL was loaded onto the stage with the gap set to 250 μm from the upper plate. Any excess material was carefully removed using a spatula, and the sample was left for 2 min to equilibrate at 37 °C. The amplitude sweep had already been carried out prior to determining the linear viscoelastic region (37 °C, 1 Hz and strains of 0.04−4%), which was then used to fix the strain of 0.2%. All radial frequency sweeps were carried out between 0.01 and 15 Hz and at a strain of 0.2%. Measurements were repeated in triplicates.

To examine stress recovery, time sweeps were carried out on the 40 mg/mL EMG-$M_{7:3}$ to simulate injection shear strain. Strain sweeps were measured at 0.2% for 5 min, followed by 1000% strain for 1 min as a simulation for injection strain, followed by 0.2% strain for 5 min, all carried out at 1 Hz frequency.

Fluorescence Microscopy. The chloroform-in-water emulsion droplets were imaged by an EVOS FL fluorescence microscope, where images were taken by an EVOS ×20 dry objective. For FITC fluorophore, excitation λ_{max} 490 nm was applied and emission λ_{max} 525 nm.

Scanning Electron Microscopy (SEM). A JCM-6000Plus Neoscope benchtop SEM was used to characterize network topology of the hydrogels as well as image the nanofibrillised microspheres formed within the EMGs. The peptide hydrogel/EMG was diluted 10-fold using HPLC water before mounting onto carbon disc, which was then either dried under vacuum or was left overnight to air-dry and sputter-coated with thin gold coating (10 nm) before imaging.

Atomic Force Microscopy (AFM). Peptide samples were diluted from hydrogels and emulgels using ddH_2O to range of concentrations (0.025 mg/mL to 0.5 mg/mL). A total of 10 μL of each dilution was dropped onto freshly cleaved mica. After 2 min, excess solution was removed, and the surface was washed once with 1 mL of HPLC grade H_2O. Excess water was then removed once again by wicking using Whatman No. 1 filter paper. The samples were allowed to air-dry for one night prior to imaging. Areas of interest were imaged by the scan-assist mode in air using a Bruker Multimode 8 atomic force microscope with a Nanoscope V controller operating under Nanoscope v8.15 software. Imaging was performed using ScanAsyst Air tips. These silicon nitride probes with Al coating have a nominal radius of curvature of about 2−5 nm and a nominal spring constant of 0.4 N m^{-1} (Bruker AXS S.A.S, France). Height images with scan sizes of either 2 μm × 2 μm or 50 μm × 50 μm were captured at a scan rate of 0.977 Hz and at a relative humidity of <40%. The instrument was periodically calibrated using a grating with 180 nm deep, 10 mm^2 depressions. Data was second-order flattened using the Nanoscope Analysis (v1.4) software prior to image export.

Transmission Electron Microscopy (TEM). A Thermo Scientific Tecnai G2 BioTwin TEM equipped with a high resolution Orius CCD SC1000 camera was used to characterize the fiber morphology of the hydrogels and EMGs at 100 keV. Samples were diluted 10-fold using HPLC grade water. A 10 μL sample was adsorbed onto the carbon-coated face of the copper grid (400 mesh); after 10 s, it was blotted away using filter papers. The grid was then washed using 10 μL of water and finally negatively stained with 10 μL of a solution of 4% (w/w) uranyl acetate. After 4 days, the samples were analyzed after being completely dried.

https://dx.doi.org/10.1021/acs.biomac.0c00366
Biomacromolecules XXXX, XXX, XXX−XXX

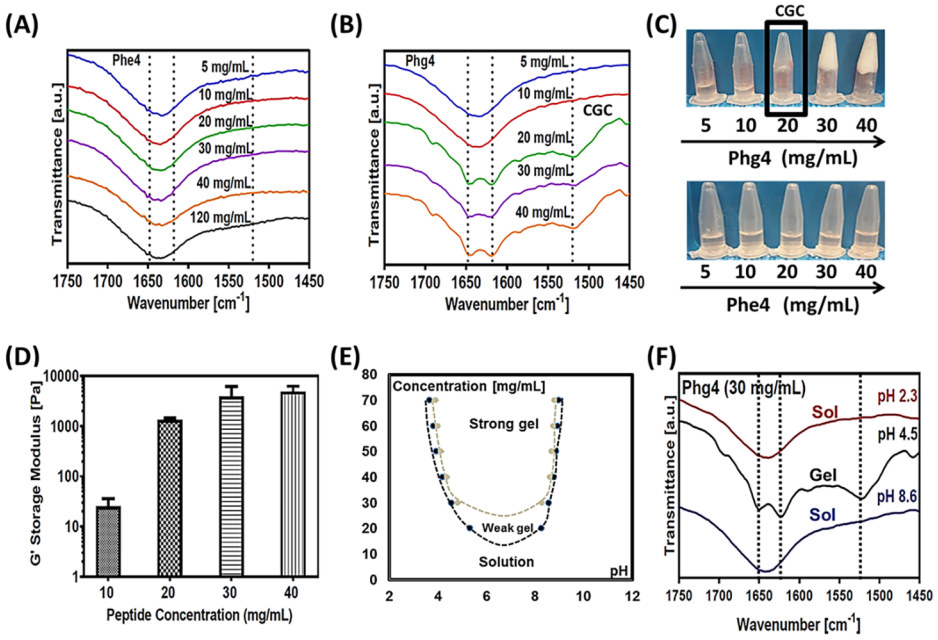

Figure 2. ATR-FTIR spectra for the two peptides: (A) Phe4 and (B) Phg4 at a series of concentrations. (C) Inverted vial test of Phg4 (top panel) and Phe4 (bottom panel) peptides at pH 5. (D) Shear modulus (G'; y-axis set to log 10) of Phg4 hydrogels at 6 rad s^{-1} obtained from the frequency sweep experiments performed at 0.2% strain. (E) Phase diagram of Phg4 peptide as a function of pH and concentration. Three distinctive states were observed: strong gel, weak gel, and solution. (F) ATR-FTIR spectra for Phg4 (30 mg/mL) showing phase transition from unstructured sol form at pH 2.3 to β-sheet gel form at pH 4.5 and back to unstructured sol form at pH 8.6.

Small Angle X-ray Scattering (SAXS). SAXS experiments were performed on beamline I22 at the Diamond Light Source (DLS) facility in Didcot, U.K. The energy of the beam was 12.4 keV corresponding to the X-ray wavelength of 0.1 nm. Quartz capillaries (1.5 mm outer diameter, 0.01 mm wall thickness) were supplied from the Capillary Tube Supplies Ltd. A total of 20 mg/mL of Phg4 hydrogel was introduced to capillaries via syringe. Acquisition time was 1 s, and the area pixel array detector used to collect SAXS data was Pilatus P3−2 M (from Dectris). The distance between samples and the detector was fixed to 2.211 m, resulting in a momentum transfer vector range of 0.086 (nm^{-1}) < q < 7.76 (nm^{-1}) with $q = (4\pi/\lambda)\sin(\theta/2)$, where θ is the scattering angle and λ is the wavelength of incident photons. Calibration of the momentum transfer was performed using silver behenate powder. ddH_2O in a capillary was used as background and subtracted from all measurements, while the subtraction mask was created using glassy carbon. Data were reduced using the processing tools at DawnDiamond software suite. The 2D scattering photon patterns were integrated using azimuthal integration tool to obtain a 1D scattering patterns.

RESULTS AND DISCUSSIONS

Self-Assembly and Gelation Properties. A phenylglycine-based ionic self-complementary tetrapeptide sequence (Phg4) was designed as a constrained analogue of the previously investigated phenylalanine-based tetrapeptide (Phe4) (Figure 1A,B).[8,9] Guilbaud et al. showed that the Phe4 sequence neither self-assembled into β-sheet nanofibers nor formed a self-supported hydrogel, as would normally be expected with ionic self-complementary sequences based on Zhang designs.[8,9] Self-assembly and gelation were only achieved by the effect of thermolysin reverse hydrolysis of Phe4 into the octapeptide FEFKFEFK at concentrations of 0.5 and 70 mg/mL, respectively.[8,9] Those findings imply that the sequence length is crucial for stability of the self-assembled β-sheet structures.

Here, the secondary structure of both Phe4 and Phg4 peptides was studied at different concentrations using ATR-FTIR at pH 4.5−5 (Figure 2A,B). As predicted from Guilbaud et al. previous findings,[8,9] the Phe4 did not show the tendency to self-assemble into β-sheet structures; instead, unstructured random conformation at all the investigated concentrations was observed, where all spectra showed a strong broad peak between 1645 and 1640 cm^{-1} (Figure 2A).[35,36] Similarly, Phg4 spectra of 5 and 10 mg/mL solution samples showed an unstructured conformation. However, 20, 30, and 40 mg/mL concentrations showed prominent peaks at 1624 and 1650 cm^{-1}, indicating hydrogen bonding between backbone amides, as well as 1524 cm^{-1} amide II band; corresponding to the formation of an extended β-sheet conformation (Figure 2B). Strikingly, Phg4 peptide showed to form self-supported cloudy hydrogel at a critical gelation concentration (CGC) ∼ 20 mg/mL (Figure 2C, top panel), which is consistent with the FTIR spectra (Figure 2B). On the other hand, Phe4 failed to form self-supported materials at the same concentration range (5−40 mg/mL; Figure 2C, bottom panel), as it lacked structure and did not self-organize into β-sheet structures (Figure 2A).

The concentration dependency of Phg4 for the sol−gel transition and mechanical properties at pH 4.5−5 were investigated using shear rheometery. The shear moduli (G') significantly increased from ∼40 Pa at 10 mg/mL to ∼1350 Pa at 20 mg/mL and ∼4500 Pa at 30 and 40 mg/mL (Figures 2D and S2A,B), showing the formation of self-supported viscoelastic hydrogels with CGC ∼ 20 mg/mL, confirming results from the inverted vial test (Figure 2C, top panel), molecular conformations (Figure 2B), and phase diagram (Figure 2E). Materials of G' 1500 Pa or slightly below were thought to be weak gels, which are self-supportive and do not flow by effect of gravity in the inverted vial test, but can be forced to flow if the tube is strongly tapped. Gels of G' > 1500 Pa are strong gels and would not flow with tapping in the

https://dx.doi.org/10.1021/acs.biomac.0c00366
Biomacromolecules XXXX, XXX, XXX−XXX

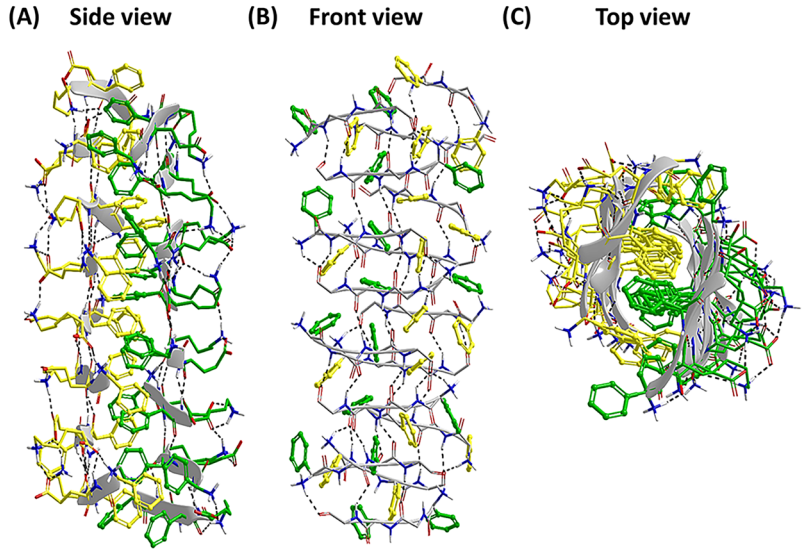

Figure 3. Predicted most stable packed dimer aggregation model from the PM7 calculations: (A) side view and (B) front view, with K and E side chains omitted to more clearly demonstrate the interchain backbone hydrogen bonding and the phenyl ring stacking interactions and (C) top view. The RMSDs between the PM7 model and the model from the initial Prime side-chain predictions were 1.5 and 2.2 Å for backbone and side chain, respectively, suggesting a good quality initial model from Prime but with PM7 theoretically more robust in terms of π-stacking optimization.[39]

inverted vial test (Figure 2E). In contrast, the shear moduli of Phe4 at the same concentrations and pH did not show the formation of stable viscoelastic hydrogel, as observed from the very low shear moduli (G') values compared to Phg4 (data not shown).

Electrostatic interactions play a key role in the self-assembly and gelation properties of β-sheet forming peptides.[37] With this in mind, we have investigated self-assembly and sol−gel phase transitions as a function of Phg4 peptide charge. To probe the charge status experimentally for comparison with theoretical calculations, peptide solution (30 mg/mL) was titrated using 0.5 M NaOH. The experimental titration curve indicates that the net peptide charge is neutral within pH range of 4.5−8 when compared to the theoretical charge curve (Figure S2C). Phase diagram of Phg4 hydrogel formation followed its symmetrical charge profile (Figures 2E and S2C) with strong hydrogels being formed at pH in the range ∼4.5−8.5, shadowing the charge profile of Phg4 peptides of neutral net charge. This agrees with Caplan and co-workers results, which suggested that a reduction in electrostatic intermolecular repulsion is required to enable stable molecular assembly of ionic self-complementary peptides.[37]

Remarkably, ATR-FTIR showed the structural switch of Phg4 from unstructured at pH 2.3 to β-sheet structure at pH 4.5 and back again to unstructured at pH 8.6, correlating well with the sol−gel−sol phase transitions and charge status, confirming that the gel formation is a result of the Phg4 self-assembly into β-sheet order (Figures 2E,F and S2C). Furthermore, fluorescence spectroscopy using Thioflavine T (ThT), which has strong binding affinity to β-sheet-like fibrils,[38] has corroborated the conformational switch of Phg4 from unstructured at pH 2.3 to β-sheet order, as indicated by the enhancement of ThT fluorescence intensity at pH 4.5, which was insignificant in the case of Phe4, indicating the unique tendency of Phg4 to self-assembly (Figure S2D).

In silico modeling was exploited to help understand at the atomic level the observed propensity of Phg4 toward self-assembly, modeled as antiparallel β-sheet ladders. Prime minimization/side chain predictions led to input models for single chain and packed dimer ladder Phg4 MD simulations. A 2 × 8 chain Phg4 dimer model was considered a good compromise between sheet length and accuracy, allowing us to postprocess MD trajectory structures using theoretically more rigorous SQM PM7 calculations that better account for potential π-stacking interactions in the aggregated assembly. The packed dimer model maintained a stable aggregation structure for the full 100 ns simulation (three independent simulations). The RMSD (system heavy atoms) was seen to stabilize after ∼10−20 ns (Figure S3) and the last 80 ns of these simulations used for further analysis. In the models, hydrophobic phenyls from both sheets were intercalated limiting exposure to solvent, and the top-to-bottom aligned charged side chains of hydrophilic K and E residues from consecutive chains formed a stable network of favorable ionic and hydrogen bond interactions throughout. The average number of interchain backbone hydrogen bonds over the three different packed dimer simulations was 2.7, 2.8, and 2.8 (overall average of 2.8). Each chain had stronger interchain hydrogen bonding on one side of the chain (averages of 3.5, 3.5, and 3.5 for the individual simulations; average when combined of 3.5) compared to the other (individual averages 1.7, 2.0 and 2.0; average when combined of 1.9). Generally at least two interchain hydrogen bonds were present throughout. We calculated an association energy for the propensity of single chains to aggregate into the models as ΔE_{assoc} (eq S1, Supporting Information) using the last 80 ns of each simulation with values of −540.3, −539.9, and −550.9 kcal mol^{-1} obtained or an average ± standard deviation of −543.7 ± 6.2 kcal mol^{-1} and indicative of significant stabilization. A video presentation of the simulation with ΔE_{assoc} = −550.9 kcal mol^{-1} is included as Supporting Information. Despite the relatively good consistency of results, we highlight that other models of aggregation are possible than these explored here and there are many possibilities (degrees of freedom) in terms of optimal π-stacking for the aggregated dimer. The PM7 optimization of the 31 trajectory cluster representatives

https://dx.doi.org/10.1021/acs.biomac.0c00366
Biomacromolecules XXXX, XXX, XXX−XXX

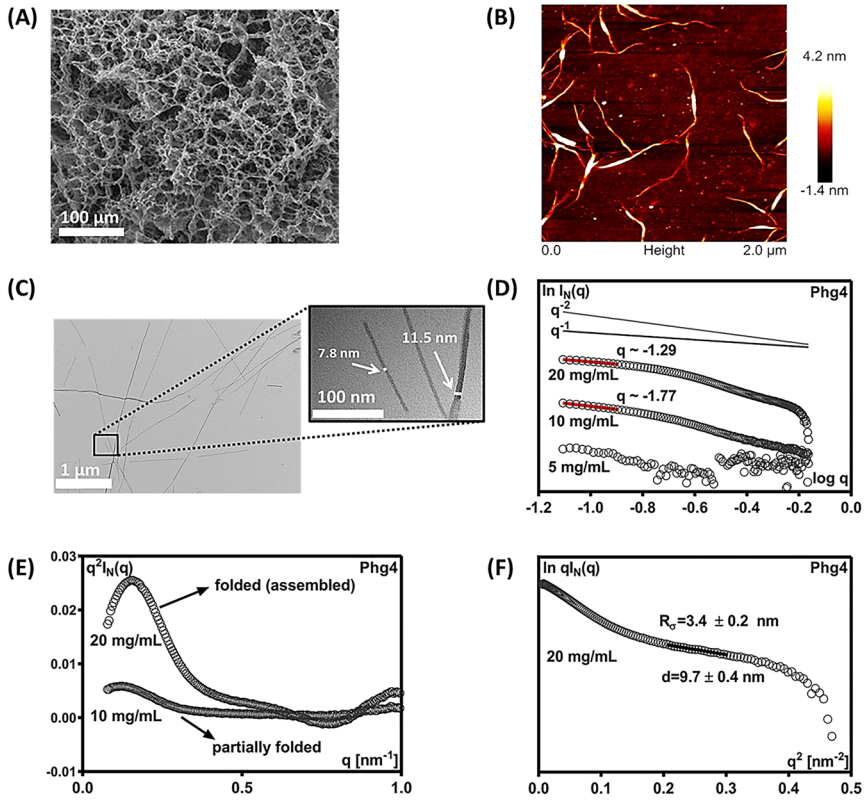

Figure 4. (A) SEM image of 10× diluted and freeze-dried Phg4 hydrogel at 30 mg/mL. (B) AFM micrographs of Phg4 hydrogel at 30 mg/mL diluted to 0.5 mg/mL. (C) TEM micrographs of 10× diluted Phg4 hydrogel at 40 mg/mL, with arrows pointing to fiber bundles of ∼7−11 nm size. (D) $\ln[I_N(q)]$ vs log q representation of SAXS of 5, 10, and 20 mg/mL of Phg4. q^{-1} and q^{-2} behavior are also presented. (E) Kratky plot ($q^2 I_N(q)$ vs q representation) of 10 and 20 mg/mL Phg4. The curve shapes are marked by arrows corresponding to folded (assembled) and partially folded states. (F) SAXS scattering pattern of a 20 mg/mL Phg4 at low q plotted in a $\ln[qIN(q)]$ vs q^2 representation.

allowed us to more closely analyze the nature of the phenyl interactions in the aggregated dimer, with the predicted most stable model based on the heats of formation shown in Figure 3A−C. The side view (Figure 3A) demonstrates the formation of a hydrophobic inner core with phenyl rings from both sheets, and the network of hydrogen bonding involving K and E side chains. The interchain backbone hydrogen bonds can also be seen but are more clearly visible in Figure 3B. Stacking and sandwich intercalation of the hydrophobic phenyl side chains from the two sheets is evident when viewed from the top (Figure 3C) and includes T-stacking and parallel-displaced π-stacking interactions (Figure 3B). The antiparallel chain arrangement allows the phenyl ring side chains of nonterminal Phg residues (*Phg*E***Phg***K) from each chain to align forming a hydrophobic central core favorable for aggregation. Predicted stabilization (from PM7/COSMO heat of formations) of the 16-chain Phg4 dimer model structure compared to free single peptide chains was considerable (−524.1 kcal mol^{-1}; relatively similar in magnitude to the ΔE_{assoc} values from the MD simulations), in further support of experiment and the packed aggregation of Phg4 chains in aqueous media. The stabilization values from PM7 optimizations can in fact be lower for other optimized frames from the MD simulations, with only MD cluster representatives used due to the computational expense involved.

On the mesoscopic scale, the ability of Phg4 peptide to form extended β-sheet nanofibrillar structures was investigated using SEM, AFM, and TEM. SEM showed a dense network of nanofibrillar structures, which is typical for hydrogel formation (Figure 4A). The AFM micrograph clearly showed slightly twisted ribbon-like morphology, which stack in a hierarchal manner to form β-sheet fibrils (Figure 4B).[40] TEM showed relatively straight long entangled nanofibers with Y-shaped branching, as well as lateral associations along the fibers length forming thicker bundles with sizes varied from ∼7−11 nm (Figure 4C). Unlike Phg4, Phe4 samples did not show any nanofibrillar structures when examined with the three microscopy techniques (data not shown).

SAXS was further used to investigate the formation and structure of the Phg4 nanofibers (Figure 4D−F). The $\ln[I_N(q)]$ versus log q representation indicated no fiber formation for 5 mg/mL, for which scattering similar to water level background was observed (Figure 4D). For 10 and 20 mg/mL samples, q values of ∼−1.77 and 1.29 were obtained, respectively (Figure 4D). Typical $\sim q^{-1}$ behavior indicating rods and $\sim q^{-2}$ indicating discs/flat objects were also plotted. As previously observed from FTIR measurements (Figure 2B), 10 mg/mL did not exhibit a structured β-sheet peak. Likewise, SAXS confirmed that at this concentration Phg4 did not assemble into a rod-like shape but random aggregates ($q \sim -1.77$), whereas at 20 mg/mL rod-like objects closely resembling fibers were observed with q value 1.29; closer to q^{-1} behavior. The slight deviation from the $q \sim -1$ behavior of 20 mg/mL, is most likely coming from the tendency of Phg4 peptide to form flattened fibers and fiber bundles through interfiber lateral growth, as observed from AFM (Figure 4B)

https://dx.doi.org/10.1021/acs.biomac.0c00366
Biomacromolecules XXXX, XXX, XXX−XXX

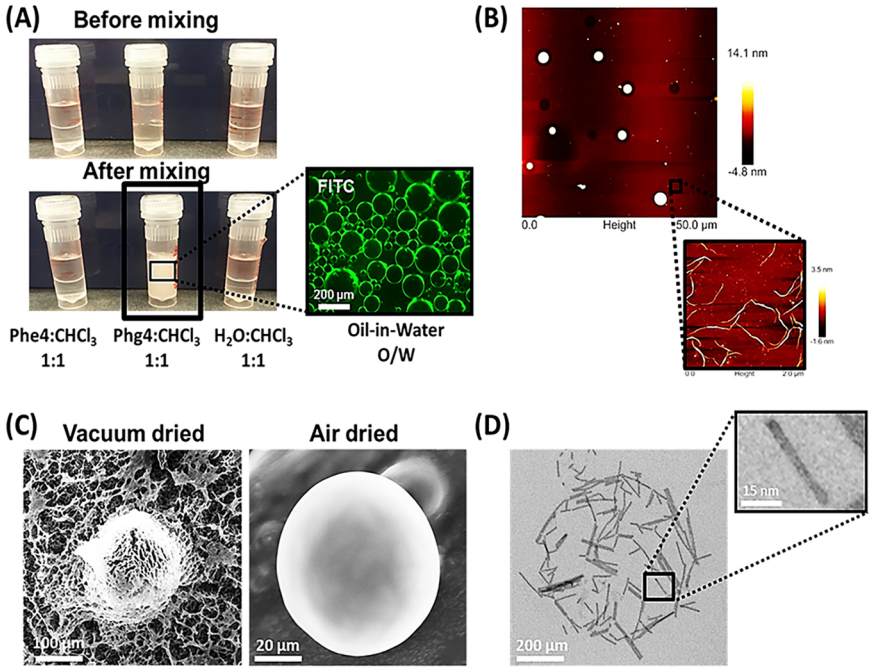

Figure 5. (A) Photograph of 20 mg/mL Phe4 and Phg4 water chloroform ($CHCl_3$) mixtures at a 1:1 volume ratio before and after mixing. Fluorescence microscopy image confirmed the formation of Phg4 oil-in-water (O/W) emulsion with the continuous aqueous phase stained with Fluorescein Isothiocyanate (FITC). (B) AFM of Phg4-$CHCl_3$ emulsion showing microspheres formed at the oil−water interface at 1:1 volume ratio after sample drying. Background region close to the sphere shows individual fibrils similar to those observed in hydrogels (Figure 3B). (C) SEM micrographs of a 30 mg/mL EMG prepared at a 1:1 W:O ratio, which has been 10× diluted and either vacuum-dried (left) or air-dried (right). (D) TEM micrographs of 10× diluted Phg4 chloroform-in-water at 30 mg/mL, showing short fiber bundles of ∼9 nm size arranged in a sphere-like shape.

and TEM (Figure 4C), respectively. In fact, Kratky plots ($q^2[I_N(q)]$ vs q) for those two concentrations showed a clear transition between partially folded structures at 10 mg/mL to fully folded (assembled) structures at 20 mg/mL (Figure 4E), respectively.[41] It has been previously shown that, for rod objects (i.e., approximately fibers), for $qR_\sigma < 1.3$ (R_σ: cross-section radius of gyration), the scattering intensity can be written as[42,43]

$$\ln qI(q) \propto -\frac{R_\sigma^{\,2}}{2}q^2 \tag{1}$$

If the scattering observed is of the form described by the above eq 1, then at low q, a linear behavior should be obtained in a $\ln[qI_N(q)]$ versus q^2 representation, which was the case with Phg4 (Figure 4F). The cross-section radius of gyration, R_σ, of the fibers can be estimated from the slope of the linear section. If the fibers can be modeled by an infinitely long cylinder, the R_σ is related to the diameter of the fiber, d, through the following equation:

$$R_\sigma = \sqrt{\frac{d^2}{8}} \tag{2}$$

By fitting the linear region, the nanofiber diameter size can be estimated as 9.7 ± 0.4 nm, which is in good agreement with the values obtained from TEM (Figure 4C). In contrary, Phe4 did not exhibit any fibril-like scattering patterns (data not shown).

The above-discussed results clearly showed the unique tendency of the ultrashort constrained Phg4 sequence to adopt stable β-sheet conformation in a concentration-dependent and pH-responsive fashion, surpassing its Phe4 counterpart that failed to self-assemble into β-sheet structure. Interestingly, the seemingly minimal change in the chemical structure had large influence on the molecular stability of self-assembly for these tetrapeptide sequences (Figure 1A,B). This is attributed to the aromatic rings orientation in Phg4, which are directly attached to the peptide sequence backbone, making them readily positioned for π-stacking stabilizing the self-assembled structure alongside the hydrogen bonds formed between backbone amides and the salt bridges between K and E residue side chains; all together forming a very stable network of noncovalent interactions from top to bottom along the fiber axis (Figure 3).

Self-Assembly and Interfacial Properties. Both Phe4 and Phg4 tetrapeptides are ionic self-complementary sequences with alternating hydrophobic and hydrophilic residue pattern (Figure 1A,B). The amphiphilic-like design suggests that both peptides can exhibit interfacial activity. To test this, the peptide aqueous phase (20 mg/mL) was mixed with chloroform as the immiscible oil phase in 1:1 volume ratio at a range of pH values. Strikingly, only Phg4 managed to form stable emulsion, but not Phe4 at pH 5 (Figure 5A). Also, both peptides showed immediate phase separation after mixing at pH 2 and 8.5 (data not shown). This implies that the surface activity is due to the adsorption of Phg4 amphiphilic nanofibers at the oil−water interface, which are formed at pH 5, rather than the monomeric nonassembled peptide chains at pH 2 or 8.5 (Figure 2F). Phe4 failed to stabilize emulsions at all pH ranges, as it does not self-assemble into amphiphilic β-sheet nanofibers. Fluorescence microscopy of Phg4 emulsion revealed the formation of oil-in-water (O/W) macroemulsion

https://dx.doi.org/10.1021/acs.biomac.0c00366
Biomacromolecules XXXX, XXX, XXX−XXX

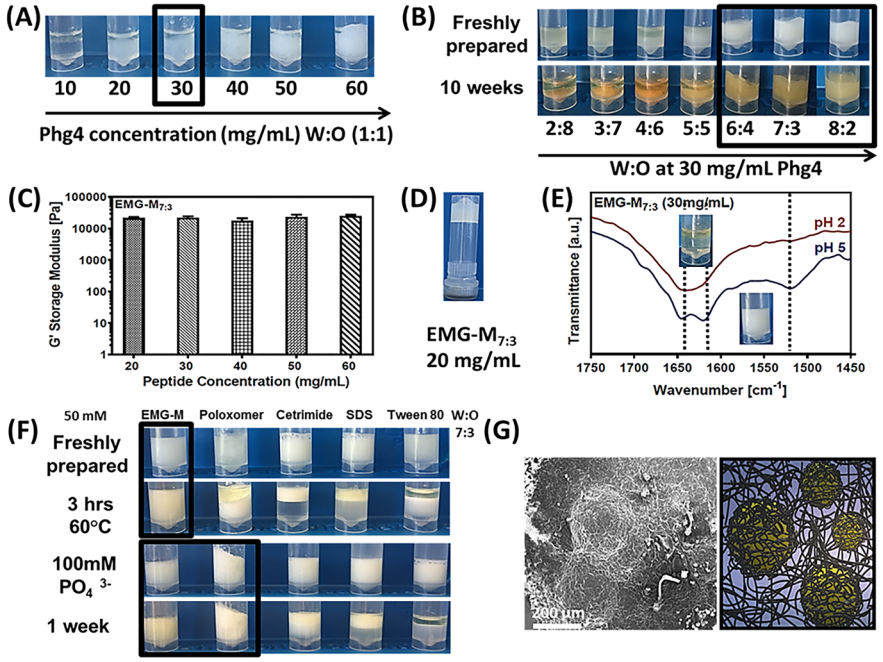

Figure 6. (A) Series of Phg4 Melissa oil mixtures with a range of peptide concentrations (10−60 mg/mL) at 1:1 W:O volume ratio. (B) EMG-M (30 mg/mL) mixed at a range of different W:O volume ratios (2:8−8:2) tested for phase separation over 10 weeks at room temperature. (C) Shear moduli (G') of EMG-$M_{7:3}$ at a range of peptide concentrations (20−60 mg/mL), performed at 6 rad s^{-1}, obtained from the frequency sweep experiments performed at 0.2% strain. (D) Inverted vial test of EMG-$M_{7:3}$ (20 mg/mL) at pH 5. (E) ATR-FTIR spectra of EMG-$M_{7:3}$ (30 mg/mL) showing phase transition from an unstructured immiscible form at pH 2 to a β-sheet structured EMG form at pH 5. (F) Emulsion stability profiles of EMG-$M_{7:3}$ vs poloxomer (Pluronic F-68), cetrimide (alkyltrimethylammonium bromide), sodium dodecyl sulfate (SDS), and tween 80 at 50 mM emulsifier concentration after incubation for 3 h at 60 °C (top panel) and after incubation with 100 mM potassium phosphate monobasic for 1 week (bottom panel). (G) Left: SEM image of EMG-$M_{7:3}$ (30 mg/mL), which has been 10× diluted and vacuum-dried, showing two oil droplets stabilized by a peptide fibrous network at the interface. Right: illustration of the O/W EMG-M showing the Melissa oil droplets in yellow entrapped within the peptide nanofibrous network suspended in the continuous aqueous hydrogel phase in blue.

(~50−200 μm) with the continuous aqueous phase stained with fluorescein isothiocyanate (FITC) green fluorescence (Figure 5A).

AFM of the dried sample revealed the formation of Phg4 microspheres surrounded with nanofibers (Figure 5B) similar to those forming hydrogels (Figure 4B), implying the formation of emulgels (EMGs). This suggests that the amphiphilic nanofibrils formed of unpacked β-sheet single ladders are adsorbed at the surface of the oil phase (chloroform) with the Phg aromatic rings oriented toward chloroform and the hydrophilic E and K residues facing the aqueous phase, by this following the "oriented wedge theory" first suggested by Harkins and Keith in the early 1900s (Figure 1C).[44,45] Based on the AFM micrograph, we also hypothesize that chloroform evaporation can lead to the formation of nanofibrilized hollow microspheres entangled within the nanofibrous network of the surrounding aqueous medium. Evidently, SEM micrograph of vacuum-dried emulsion clearly showed the formation of nanofibrilized porous microspheres within the nanofibrous network of the continuous phase, while the air-dried sample showed the formation of solid peptide microspheres (Figure 5C). It is worth mentioning here that artifacts could happen from sample preparation, where it was observed that the nanofibrous network surrounding microspheres was slightly cracked from vacuum drying (Figure 5C, left micrograph). In general, Phg4 microspheres showed similar morphology in SEM to the Fmoc-YL that was previously reported by Ulijn and co-workers to stabilize chloroform-in-water emulsions,[16] as well as the surfactant-like decapeptide A_9R that was reported by Hamley and co-workers to stabilize water-in-1-bromohexadecane emulsions.[19] The TEM micrograph of diluted emulsion manifested short β-sheet fiber bundles adopting spherical arrangement with bundle diameter size of ~9 nm (Figure 5D), which is within the size range of the hydrogel forming fibers (Figure 4C,F).

Phg4 Peptide Emulgels (EMG). We have then changed the oil phase from chloroform to the pharmaceutically relevant and more viscous oil phase, Melissa oil, which is extracted from the leaves of Melissa officinalis species of the Lamiaceae family. It has been reported that Melissa oil possesses antimicrobial,[46] antifungal,[47] antiviral,[48] and antioxidant[49] activities. The Phg4-based O/W emulgels with Melissa as the oil phase (EMG-M) has been formulated by simple mixing of oil droplets in the peptide aqueous phase at self-assembly pH 5. First, the effect of Phg4 peptide concentration on the formulation stability was studied at 1:1 W:O ratio. No emulsion formation was observed at 10 mg/mL, but at 20 mg/mL emulsions were obtained with minimal phase separation observed at concentrations ≥30 mg/mL (Figure 6A). This correlates with the FTIR spectra, where Phg4 was unstructured at 10 mg/mL and acquired the β-sheet structure at 20 mg/mL, where self-assembly into the emulsifying amphiphilic β-sheet ladders occurs (Figure S4A).

The effect of the W:O ratio on the formulation stability was evaluated at 30 mg/mL peptide concentration. After 10 weeks of storage, we noticed that increasing the water volume above 50% yielded the most stable formulations (Figure 6B). Indeed, FTIR spectroscopy confirmed these visual observations with strong β-sheet peak at ~1624 cm^{-1} for W:O ratios 6:4, 7:3,

https://dx.doi.org/10.1021/acs.biomac.0c00366
Biomacromolecules XXXX, XXX, XXX−XXX

and 8:2 (Figure S4B). Shear rheology confirmed the formation of viscoelastic hydrogel-like system for W:O 7:3 samples at a range of peptide concentrations (20−60 mg/mL) with shear moduli ∼20 kPa (Figures 6C and S5A,B). The high stiffness of EMG-M, as indicated from G' values, compared to hydrogels of G' hundreds Pa (Figures 2D and S2B) could be attributed to network structure changes associated with the formation of nanofibrillised microspheres; which could have enhanced the mechanical strength of the nanofibrous network of the continuous aqueous phase. The EMG-M stiffness was not significantly affected by the W:O ratio (Figure S5C). Also, EMG-M formulation showed to be not only shear-thinning, but also pseudoplastic thixotropic, where instantaneous, but partial recovery from shear strain was observed from the controlled strain profile of EMG-$M_{7:3}$ at 40 mg/mL Phg4 concentration (Figure S5D). This implicates the injectability of these peptide emulgels (Figure S5D), where fast recovery kinetics is a desirable parameter to avoid uncontrolled release of cargos post injection; which is a useful material property for drug and cell delivery applications. Inverted vial test revealed a CGC for a self-supported emulsion-gel or "emulgel" (EMG) system of ∼20 mg/mL for a 7:3 W:O ratio (Figure 6D), similar to that observed for the hydrogel formulations (Figure 2C, top panel).

The stability profile of EMG-$M_{7:3}$ (30 mg/mL) formulation was studied under various physical, chemical, and environmental conditions. The EMG-M stability was indeed affected by pH, where the colloidal system was most stable at the self-assembly pH 5 due to the formation of the emulsifier amphiphilic β-sheet ladders (Figure 6E). Phase separation was observed at pH 2 (Figure 6E) and 8.5 (data not shown), as the peptide is unstructured at these pH values (Figures 2F and 6E). The correlation of structural and phase transitions suggests that the amphiphilic nanofibers are the effective emulsifier and not the nonassembled individual peptide chains. Over long storage (up to 5 weeks), EMG-M showed to be more stable, compared to a variety of commercial surfactants belonging to different classes of surface active agents and commonly used in pharmaceutical and cosmetic products such as the cationic surfactant cetrimide (alkyltrimethylammonium bromide), the anionic sodium dodecyl sulfate (SDS), and the nonionic tween 80 that all showed phase separation when used at the same concentration (50 mM; Figure S6A). However, only the nonionic surfactant poloxomer (Pluronic F-68) showed similar stabilization as EMG-M, as both formed a self-supported hydrogel that helped stabilize suspended oil droplets through the highly viscous continuous phase (Figure S6A). EMG-M was the only formulation that showed thermal stability when heated for 3 h at 60 °C, while phase separation occurred with all other emulsifiers, including poloxomer (Figure 6F, top panel). The salting-out effect was studied as well, using a variety of salts (phosphate, chloride and thiocyanate), and in all cases, only EMG-M and poloxomer emulsions were shown to be stable for one week (Figure 6F, bottom panel, and Figure S6B). Ulijn and co-workers have also reported the ability of the β-sheet forming Fmoc-capped short aromatic sequences to stabilize chloroform-in-water emulsions for 24 h better than SDS when incubated with phosphate, chloride, and thiocyanate salts.[16]

SEM of diluted EMG-M showed peptide nanofibrils adsorbed at the oil−water interface and surrounding the oil droplets (Figure 6G, left panel). This confirms the stabilization of the EMG system through formation of amphiphilic nanofibers that not only adsorb at the oil−water interface, but also form a fibrous network that helps stabilize the system by entrapping the suspended oil droplets within the highly viscous hydrogel continuous phase (Figure 6G, right panel).

Our results, therefore, have demonstrated the considerable potential of using Phg4 amphiphilic nanofibers as emulsifiers in pharmaceutical, cosmetics, and food industries, as it overcomes the major limitation of commercial surfactants; the instability toward environmental and storage conditions.

CONCLUSION

To the best of our knowledge, we have reported for the first time the shortest ionic self-complementary sequence (Phg4 tetrapeptide) that self-assembles into stable amphiphilic β-sheet nanofibers capable of gelation and emulsification. This was achieved by the rational design of a constrained tetrapeptide analogue of the previously reported nonassembling Phe4, exploiting the properties of a more rigid phenylglycine residue. We hypothesized the atomistic interactions leading to stability of self-assembled fibrils through hybrid molecular dynamics simulations and SQM calculations, which highlighted the strong potential for favorable aggregation through π-stacking interactions involving the aromatic Phg side chains from different sheets. These fibrils showed both the ability to form hydrogels in monophasic aqueous medium and interfacial activity in biphasic media forming stable emulgels. Our results highlight the importance of complementary interfacial noncovalent forces alongside backbone amide hydrogen bonding to stabilize the molecular self-assembly of short peptides as exemplified by favorable aromatic stacking in this study. Ultrashort ionic-complementary constrained peptides or UICPs have significant potential for the development of cost-effective, sustainable, and multifunctional soft nanomaterials based on robust nanoassemblies possessing both hydrogelation and emulsification properties: beneficial attributes for the development of a wide range of materials for biomedical, pharmaceutical, cosmetic, and food applications.

ASSOCIATED CONTENT

Supporting Information

The Supporting Information is available free of charge at https://pubs.acs.org/doi/10.1021/acs.biomac.0c00366.

Molecular dynamics details, HPLC chromatograms of used peptides, additional oscillatory rheology data for hydrogels and emulgels (strain sweep, frequency sweep, and strain recovery), theoretical net charge and titration curve of Phg4 peptide, ThT fluorescence for the two peptides, additional ATR-FTIR for emulgel EMG-M (different peptide concentrations and W:O ratios), and emulsion stability profiles for EMG-M compared to commercial emulsifiers (PDF)

Molecular dynamics simulation video for Phg4 packed dimer (MP4)

AUTHOR INFORMATION

Corresponding Author

Mohamed A. Elsawy − *School of Materials, University of Manchester, Manchester M13 9PL, United Kingdom; Manchester Institute of Biotechnology, Manchester M13 9PL, United Kingdom; School of Pharmacy and Biomedical Sciences, University of Central Lancashire, Preston PR1 2HE, United Kingdom; Leicester Institute of Pharmaceutical Innovation,*

https://dx.doi.org/10.1021/acs.biomac.0c00366
Biomacromolecules XXXX, XXX, XXX−XXX

Leicester School of Pharmacy, De Monfort University, Leicester LE1 9BH, United Kingdom; orcid.org/0000-0003-3964-2150; Phone: +44(0)1163664581; Email: mohamed.elsawy@dmu.ac.uk

Authors

Jacek K. Wychowaniec − *School of Materials, University of Manchester, Manchester M13 9PL, United Kingdom; Manchester Institute of Biotechnology, Manchester M13 9PL, United Kingdom; School of Chemistry, University College Dublin, Dublin, Ireland;* orcid.org/0000-0002-6597-5242

Ronak Patel − *School of Pharmacy and Biomedical Sciences, University of Central Lancashire, Preston PR1 2HE, United Kingdom*

James Leach − *School of Pharmacy and Biomedical Sciences, University of Central Lancashire, Preston PR1 2HE, United Kingdom*

Rachel Mathomes − *School of Pharmacy and Biomedical Sciences, University of Central Lancashire, Preston PR1 2HE, United Kingdom*

Vikesh Chhabria − *School of Pharmacy and Biomedical Sciences, University of Central Lancashire, Preston PR1 2HE, United Kingdom*

Yogita Patil-Sen − *School of Pharmacy and Biomedical Sciences, University of Central Lancashire, Preston PR1 2HE, United Kingdom*

Araida Hidalgo-Bastida − *Centre for Biosciences, Department of Life Science, Centre for Musculoskeletal Science and Sports Medicine, and Centre for Advance Materials and Surface Engineering, Manchester Metropolitan University, Manchester M1 5GD, United Kingdom*

Robert T. Forbes − *School of Pharmacy and Biomedical Sciences, University of Central Lancashire, Preston PR1 2HE, United Kingdom*

Joseph M. Hayes − *School of Pharmacy and Biomedical Sciences, University of Central Lancashire, Preston PR1 2HE, United Kingdom;* orcid.org/0000-0002-7745-9616

Complete contact information is available at: https://pubs.acs.org/10.1021/acs.biomac.0c00366

Notes

The authors declare no competing financial interest.

■ ACKNOWLEDGMENTS

The authors are grateful to the School of Pharmacy and Biomedical Sciences at University of Central Lancashire (UCLan) for funding this work through the start-up fund awarded to M.A.E. and the Graduate Internship awarded to J.L. Authors would like to thank Prof. Alberto Saiani from School of Materials, University of Manchester (UoM) for his support and scientific discussions of SAXS data analysis. Authors are grateful to the staff in JB Firth analytical suite at UCLan for their assistance and training R.P. and J.L. on how to use SEM. Authors also acknowledge the Engineering and Physical Sciences Research Council (EPSRC) for supporting the work of J.K.W. of the Northwest Nanoscience Doctoral Training Centre (NOWNANO DTC), with an EP/G03737X/1 Grant, and an EPSRC Doctoral Training Award (DTA) from the School of Materials, UoM. Authors would like to thank the staff in the EM facility in the Faculty of Biology, Medicine and Health, of the UoM, for their assistance, and the Welcome Trust for equipment grant support to the EM facility. The authors are grateful to Dr. Nigel Hodson (UoM) for his assistance with the AFM experiments, Xinyi Zhu (UoM) for training R.P. on TEM sample preparation, and Diamond Light Source for the Beam Time Award (SM17102) to M.A.E. and J.K.W. and the staff on Beamline I22 for their support with the SAXS experiments, in particular, Andrew J. Smith. Authors would also like to thank Nadia Moinuddin (UCLan) for acquiring preliminary data on chloroform-in-water emulsions funded by UCLan Undergraduate Research Internship Scheme (URIS).

■ REFERENCES

(1) Mandal, D.; Nasrolahi Shirazi, A.; Parang, K. Self-assembly of peptides to nanostructures. *Org. Biomol. Chem.* **2014**, *12* (22), 3544−3561.

(2) Panda, J. J.; Chauhan, V. S. Short peptide based self-assembled nanostructures: implications in drug delivery and tissue engineering. *Polym. Chem.* **2014**, *5* (15), 4431−4449.

(3) Zhang, S.; Lockshin, C.; Cook, R.; Rich, A. Unusually stable β-sheet formation in an ionic self-complementary oligopeptide. *Biopolymers* **1994**, *34* (5), 663−672.

(4) Zhang, S. G.; Holmes, T.; Lockshin, C.; Rich, A. Spontaneous assembly of a self-complementary oligopeptide to form a stable macroscopic membrane. *Proc. Natl. Acad. Sci. U. S. A.* **1993**, *90* (8), 3334−3338.

(5) Zhang, S.; Lockshin, C.; Herbert, A.; Winter, E.; Rich, A. Zuotin, a putative Z-DNA binding protein in *Saccharomyces cerevisiae*. *EMBO J.* **1992**, *11* (10), 3787−3796.

(6) Elsawy, M. A.; Smith, A. M.; Hodson, N.; Squires, A.; Miller, A. F.; Saiani, A. Modification of beta-sheet forming peptide hydrophobic face: effect on self-assembly and gelation. *Langmuir* **2016**, *32* (19), 4917−4923.

(7) Gao, J.; Tang, C.; Elsawy, M. A.; Smith, A.; Miller, A.; Saiani, A. Controlling self-assembling peptide hydrogel properties through network topology. *Biomacromolecules* **2017**, *18* (3), 826−834.

(8) Guilbaud, J.-B.; Vey, E.; Boothroyd, S.; Smith, A. M.; Ulijn, R. V.; Saiani, A.; Miller, A. F. Enzymatic catalyzed synthesis and triggered gelation of ionic peptides. *Langmuir* **2010**, *26* (13), 11297−11303.

(9) Guilbaud, J.-B.; Rochas, C.; Miller, A. F.; Saiani, A. Effect of Enzyme Concentration of the Morphology and Properties of Enzymatically Triggered Peptide Hydrogels. *Biomacromolecules* **2013**, *14* (5), 1403−1411.

(10) Yokoi, H.; Kinoshita, T.; Zhang, S. Dynamic reassembly of peptide RADA16 nanofiber scaffold. *Proc. Natl. Acad. Sci. U. S. A.* **2005**, *102* (24), 8414−8419.

(11) Swanekamp, R. J.; DiMaio, J. T. M.; Bowerman, C. J.; Nilsson, B. L. Coassembly of enantiomeric amphipathic peptides into amyloid-inspired rippled β-sheet fibrils. *J. Am. Chem. Soc.* **2012**, *134* (12), 5556−5559.

(12) Bowerman, C. J.; Nilsson, B. L. Review self-assembly of amphipathic β-sheet peptides: Insights and applications. *Biopolymers* **2012**, *98* (3), 169−184.

(13) Lee, N. R.; Bowerman, C. J.; Nilsson, B. L. Effects of varied sequence pattern on the self-assembly of amphipathic peptides. *Biomacromolecules* **2013**, *14* (9), 3267−3277.

(14) Gazit, E. A possible role for π-stacking in the self-assembly of amyloid fibrils. *FASEB J.* **2002**, *16* (1), 77−83.

(15) Li, J.; Du, X. W.; Hashim, S.; Shy, A.; Xu, B. Aromatic-Aromatic interactions enable alpha-helix to beta-sheet transition of peptides to form supramolecular hydrogels. *J. Am. Chem. Soc.* **2017**, *139* (1), 71−74.

(16) Bai, S.; Pappas, C.; Debnath, S.; Frederix, P. W. J. M.; Leckie, J.; Fleming, S.; Ulijn, R. Stable Emulsions Formed by Self-Assembly of Interfacial Networks of Dipeptide Derivatives. *ACS Nano* **2014**, *8* (7), 7005−7013.

(17) Moreira, I. P.; Sasselli, I. R.; Cannon, D. A.; Hughes, M.; Lamprou, D. A.; Tuttle, T.; Ulijn, R. V. Enzymatically activated

emulsions stabilised by interfacial nanofibre networks. *Soft Matter* **2016**, *12* (9), 2623−2631.
(18) Aviño, F.; Matheson, A. B.; Adams, D. J.; Clegg, P. S. Stabilizing bubble and droplet interfaces using dipeptide hydrogels. *Org. Biomol. Chem.* **2017**, *15* (3), 6342−6348.
(19) Castelletto, V.; Edwards-Gayle, C. J. C.; Hamley, I. W.; Barrett, G.; Seitsonen, J.; Ruokolainen, J. Peptide-stabilized emulsions and gels from an arginine-rich surfactant-like peptide with antimicrobial activity. *ACS Appl. Mater. Interfaces* **2019**, *11* (10), 9893−9903.
(20) Schrodinger Release 2016−3, Schrodinger LLC, New York, NY, 2016.
(21) Olsson, M. H.; Søndergaard, C. R.; Rostkowski, M.; Jensen, J. H. PROPKA3: Consistent treatment of internal and surface residues in empirical pKa predictions. *J. Chem. Theory Comput.* **2011**, *7* (2), 525−537.
(22) McGaughey, G. B.; Gagne, M.; Rappe, A. K. π-stacking interactions alive and well in proteins. *J. Biol. Chem.* **1998**, *273* (25), 15458−15463.
(23) Hayes, J. M.; Greer, J. C.; Morton-Blake, D. A. A force-field description of short-range repulsions for high density alkane molecular dynamics simulations. *J. Comput. Chem.* **2004**, *25* (16), 1953−1966.
(24) Jacobson, M. P.; Friesner, R. A.; Xiang, Z.; Honig, B. On the role of the crystal environment in determining protein side-chain conformations. *J. Mol. Biol.* **2002**, *320* (3), 597−608.
(25) Harder, E.; Damm, W.; Maple, J.; Wu, C.; Reboul, M.; Xiang, J. Y.; Wang, L.; Lupyan, D.; Dahlgren, M. K.; Knight, J. L.; Kaus, J. W.; Cerutti, D. S.; Krilov, G.; Jorgensen, W. L.; Abel, R.; Friesner, R. A. OPLS3: A Force Field Providing Broad Coverage of Drug-like Small Molecules and Proteins. *J. Chem. Theory Comput.* **2016**, *12* (1), 281−296.
(26) Li, J.; Abel, R.; Zhu, K.; Cao, Y.; Zhao, S.; Friesner, R. A. The VSGB 2.0 model: a next generation energy model for high resolution protein structure modelling. *Proteins: Struct., Funct., Genet.* **2011**, *79* (10), 2794−2812.
(27) *Desmond Molecular Dynamics System*; D. E. Shaw Research: New York, NY, 2016.
(28) Frey, B. J.; Dueck, D. Clustering by passing messages between data points. *Science* **2007**, *315* (5814), 972−976.
(29) Stewart, J. J. P. Optimization of parameters for semiempirical methods VI: more modifications to the NDDO approximations and re-optimization of parameters. *J. Mol. Model.* **2013**, *19* (1), 1−32.
(30) Klamt, A.; Schüürmann, G. COSMO: a new approach to dielectric screening in solvents with explicit expressions for the screening energy and its gradient. *J. Chem. Soc., Perkin Trans. 2* **1993**, *2* (5), 799−805.
(31) Klamt, A.; Moya, C.; Palomar, J. A comprehensive comparison of the IEFPCM and SS(V)PE continuum solvation methods with the COSMO approach. *J. Chem. Theory Comput.* **2015**, *11* (9), 4220−4225.
(32) Høyvik, I.-M.; Jansik, B.; Jørgensen, P. Trust region minimization of orbital localization functions. *J. Chem. Theory Comput.* **2012**, *8* (9), 3137−3146.
(33) Lehtola, S.; Jónsson, H. Unitary optimization of localized molecular orbitals. *J. Chem. Theory Comput.* **2013**, *9* (12), 5365−5372.
(34) Stewart, J. J. P. MOPAC2016, Version 18.270L, 2016, website: http://OpenMOPAC.net.
(35) Barth, A. Infrared spectroscopy of proteins. *Biochim. Biophys. Acta, Bioenerg.* **2007**, *1767* (9), 1073−1101.
(36) Barth, A.; Zscherp, C. What vibrations tell us about proteins. *Q. Rev. Biophys.* **2002**, *35* (4), 369−430.
(37) Caplan, M. R.; Moore, P. N.; Zhang, S. G.; Kamm, R. D.; Lauffenburger, D. A. Self-assembly of a beta-sheet protein governed by relief of electrostatic repulsion relative to Van der Waals attraction. *Biomacromolecules* **2000**, *1* (4), 627−631.
(38) Maskevich, A. A.; Stsiapura, V. I.; Kuzmitsky, V. A.; Kuznetsova, I. M.; Povarova, O. I.; Uversky, V. N.; Turoverov, K. K. Spectral properties of thioflavin t in solvents with different dielectric properties and in a fibril-incorporated form. *J. Proteome Res.* **2007**, *6* (4), 1392−1401.
(39) Yilmazer, N. D.; Korth, M. Enhanced semiempirical QM methods for biomolecular interactions. *Comput. Struct. Biotechnol. J.* **2015**, *13* (2015), 169−175.
(40) Davies, R. P. W.; Aggeli, A.; Beevers, A. J.; Boden, N.; Carrick, L. M.; Fishwick, C. W. G.; Mcleish, T. C. B.; Nyrkova, I.; Semenov, A. N. Self-assembling β-sheet tape forming peptides. *Supramol. Chem.* **2006**, *18* (5), 435−443.
(41) Mertens, H. D.; Svergun, D. I. Structural characterization of proteins and complexes using small-angle X-ray solution scattering. *J. Struct. Biol.* **2010**, *172* (1), 128−141.
(42) Wychowaniec, J. K.; Iliut, M.; Zhou, M.; Moffat, J.; Elsawy, M.; Pinheiro, W.; Hoyland, J.; Miller, A.; Vijayaraghavan, A.; Saiani, A. Designing peptide/graphene hybrid hydrogels through fine-tuning of molecular interactions. *Biomacromolecules* **2018**, *19* (7), 2731−2741.
(43) Guilbaud, J.-B.; Saiani, A. Using small angle scattering (SAS) to structurally characterise peptide and protein self-assembled materials. *Chem. Soc. Rev.* **2011**, *40* (3), 1200−1210.
(44) Harkins, W. D.; Davies, E. C. H.; Clark, G. L. The orientation of molecules in the surfaces of liquids, the energy relations at surfaces, solubility, adsorption, emulsification, molecular association and the effect of acids and bases on interfacial tension. (Surface energy VI). *J. Am. Chem. Soc.* **1917**, *39* (4), 541−596.
(45) Harkins, W. D.; Keith, E. B. The oriented wedge theory of emulsions and the inversion of emulsions. *Science* **1924**, *59* (1534), 463−467.
(46) Mimica-Dukic, N.; Bozin, B.; Sokovic, M.; Simin, N. Antimicrobial and antioxidant activities of Melissa officinalis L. (Lamiaceae) essential oil. *J. Agric. Food Chem.* **2004**, *52* (9), 2485−2489.
(47) Serra, E.; Hidalgo-Bastida, L. A.; Verran, J.; Williams, D.; Malic, S. Antifungal Activity of Commercial Essential Oils and Biocides against *Candida albicans*. *Pathogens* **2018**, *7* (1), 1−12.
(48) Schnitzler, P.; Schuhmacher, A.; Astani, A.; Reichling, J. Melissa officinalis oil affects infectivity of enveloped herpesviruses. *Phytomedicine* **2008**, *15* (9), 734−740.
(49) Angelini, P.; Tirillini, B.; Akhtar, M. S.; Dimitriu, L.; Bricchi, E.; Bertuzzi, G.; Venanzoni, R. Essential Oil with Anticancer Activity: An Overview. In *Anticancer Plants: Natural Products and Biotechnological Implements*; Akhtar, M. S.; Swamy, M. K., Eds.; Springer: Singapore, 2018; Vol. *2*, pp 207−231.

https://dx.doi.org/10.1021/acs.biomac.0c00366
Biomacromolecules XXXX, XXX, XXX−XXX